NON LINEAR EVOLUTION OF ALFVÉN WAVES IN THE SOLAR ATMOSPHERE

A. Verdini[(1)], M. Velli[(1),(2)], and S. Oughton[(3)]

[(1)]*Dipartimento di Astronomia e Scienza dello Spazio, Firenze, Italy*
[(2)]*Jet Propulsion Laboratory, California Instiute of Technology, Pasadanea 91109, CA*
[(3)]*Department of Mathematics, University of Waikato, Private Bag 3105, Hamilton, New Zeland*

ABSTRACT

We investigate the non-linear evolution of Alfvén waves in the solar atmosphere and wind, from the photosphere out to the Earth's orbit. Photosphere and chromosphere are modeled as isothermal layers in static equilibrium, connecting across the transition region with a corona and wind. Nonlinear coupling between waves propagating in opposite directions is modeled by a phenomenological term containing an integral turbulent length scale. Spectrum modifications remain similar to what is found in a linear analysis and some characteristic features - i.e. oscillations at higher frequencies- persist despite nonlinear interactions.

1. INTRODUCTION

In situ measurements of magnetic and velocity field fluctuations from Helios and Ulysses have revealed a broad developed spectrum for frequencies ranging from $10^{-4}\ Hz$ to $10^{-2}\ Hz$ (for the fast component of the solar wind). Typically, a strong correlation between magnetic field and velocity fluctuations in this distance range persists (Mangeney et al. 1991) corresponding to an outwardly propagating spectrum. It is well known that nonlinear terms couple Alfvén waves propagating in opposite directions whereas one expects waves from the sun to propagate only outward. A question which naturally arises therefore concerns the drivers for the nonlinear cascade in this outwardly dominant case. In the solar wind, it appears that compressible processes (e.g. parametric decay) or interactions with the solar wind structure (high and low speed streams, micro-streams) may be responsible. What originates the well developed spectrum in the outward waves already seen at 0.3 AU?

Wave propagation has been extensively studied in the linear case (Heinemann & Olbert 1980; Leroy 1980; Mangeney et al. 1991; Velli et al. 1991; Velli 1993; Hollweg 1978; Similon & Zargham 1992; Lou & Rosner 1994. Dmitruk et al. 2001b developed a phenomenological non linear model based on the idea of wave reflection. The dynamics of a well developed turbulent state in the expanding solar wind has been studied as well and and an ordering of the characteristic time scale which should effectively favor the development of a turbulent cascade in planes perpendicular to the direction of wave propagation (along the magnetic field) has been found (Zank et al. 1996; Matthaeus et al. 1998, 1999; Dmitruk et al. 2001a, 2002; Dmitruk & Matthaeus 2003; Oughton et al. 2001, 2004).

The aim of this paper is to investigate reflection-generated nonlinear effects on wave propagation and frequency-spectrum modification once the background medium gradients are taken into account throughout the entire atmosphere. Following Dmitruk et al. 2001b, we choose a transverse dissipative length scale but we introduce frequency coupling to for the account energy redistribution inside the spectrum.

2. THE MODEL

The equations describing the propagation of Alfvén waves in an in-homogeneous stationary medium can be derived from the Magnetohydrodynamic equations (MHD) under the hypotheses of incompressible transverse fluctuations. The velocity $(\mathbf{u})$ and magnetic field fluctuations $(\mathbf{b})$ can be combined to form the Elsässer variables $\mathbf{z}^{\pm} = \mathbf{u} \mp sign(\mathbf{B_0})\mathbf{b}/\sqrt{4\pi\rho}$ which describe Alfvén waves propagating outward $(\mathbf{z}^{+})$ or inward $(\mathbf{z}^{-})$. $\mathbf{B_0}$ is the average magnetic field while ρ is the density of the ambient medium. In terms of these variables the equations for the two fields read:

$$\frac{\partial \mathbf{z}^{\pm}}{\partial t} + [(\mathbf{U} \pm \mathbf{V_a}) \cdot \boldsymbol{\nabla}]\mathbf{z}^{\pm} + (\mathbf{z}^{\mp} \cdot \boldsymbol{\nabla})(\mathbf{U} \mp \mathbf{V_a}) +$$

$$+\frac{1}{2}(\mathbf{z}^{-} - \mathbf{z}^{+})[\boldsymbol{\nabla} \cdot \mathbf{V_a} \mp \frac{1}{2}(\boldsymbol{\nabla} \cdot \mathbf{U})] = -(\mathbf{z}^{\mp} \cdot \boldsymbol{\nabla})\mathbf{z}^{\pm} \quad (1)$$

where $\mathbf{U}$ is the mean wind speed and the Alfvén speed is $\mathbf{V_a} = \mathbf{B_0}/\sqrt{4\pi\rho}$, co-linearity between magnetic and gravitational field is assumed. On the right hand side we have grouped the nonlinear terms (except the total pressure, which in the limit of incompressible fluctuations can also be written as products of $\mathbf{z}^{+}$, $\mathbf{z}^{-}$ and their gradients). In the linear part of the eq.1 we can recognize a propagation term (II) and two terms accounting for reflection due to the variation of the properties of the medium, one isotropic (IV) while the other (III) involves variations along the fluctuation polarization.

The cromosphere and the photosphere are modeled as a static atmosphere, $2400\ \mathrm{km}$ thick, in supra-spherical geometry with constant temperature. The density varies almost exponentially and the magnetic field varies according to the flux tube expansion (A) modeled to reproduce the properties of a coronal hole in the quiet Sun (Hollweg et al. 1982). Across the transition region the density falls off by two orders of magnitude, the wind passes from a speed of $0\ \mathrm{km/s}$ to $8\ \mathrm{km/s}$ while the magnetic

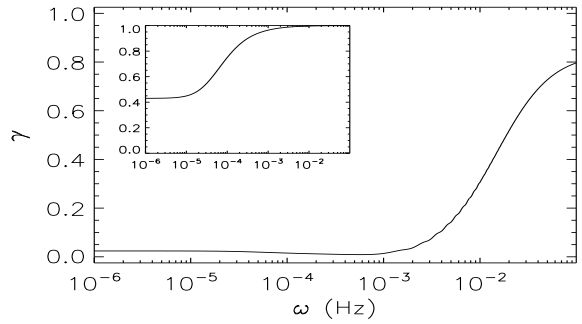

Figure 1. Dissipation efficiency (γ) as function of frequency. Inset: γ for the subalfvénic Corona (from $1\ R_\odot$ to $\approx 13\ R_\odot$); main figure, γ for the photosphere-cromosphere layer (from 2400 km below the Sun's surface to the Transition Region).

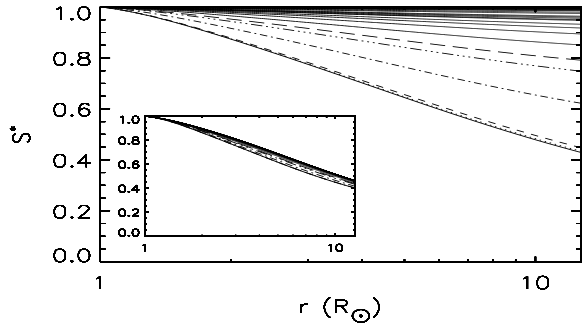

Figure 2. Total wave action density normalized to its value at the base of the Corona ($1\ R_\odot$) as function of distance for the 32 frequencies used to describe the spectrum. In the main figure the result is shown for nonlinear interaction which are local in the frequency space (model A), while in the subfigure the interaction with the whole spectrum is considered (model B). The frequency increases from the bootm curve to the top curve.

field strength is continuous (about 10 G). The corona also expands supra-spherically and its temperature profile is chosen to fit observations: 8×10^5 K at the coronal base, peaks at about 3×10^6 K at $3\ R_\odot$ and then falls off with distance as $R^{-0.8}$ (Casalbuoni et al. 1999). The wind speed profile follows from the wind equations with given temperature and flux tube expansion, of the form $A(r) = f(r)r^2$, with f a function which has a maximum close to the coronal base and tends to 1 at large distances (see Kopp & Holzer 1976, and Munro & Jackson 1977). The same functional form is chosen for the expansion in the static part of the atmosphere but different parameters are selected in order to obtain realistic values for the magnetic field and its continuos variation at the transition region. In the photosphere and cromosphere the profile for Alfvén speed is obtained from the magnetic flux conservation, $B = B_0 A_0 / A(r)$, and the density profile imposed.

Following Dmitruk et al. (2001b) we choose the follow-

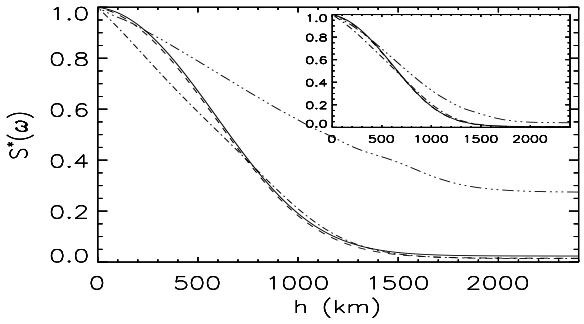

Figure 3. Energy flux normalized to its value at the base of the Photosphere (2400 km below the Sun surface) as function of distance. Only 4 representative frequencies (among the 32 forming the spectrum) are plotted: 10^{-6} Hz solid line, 10^{-4} Hz dashed line, 10^{-3} Hz dotted-dashed line, 10^{-2} Hz triple dotted-dashed line. The main figure shows the plot for the model A, while the subfigure shows results for the model B.

ing model for the nonlinear terms in eq.(1)

$$NL_j^{\pm} = \mathbf{z}^{\pm}(\omega_j)\frac{|\mathbf{Z}^{\mp}|}{L(r)} \tag{2}$$

where L represents an integral turbulent dissipation length and $\mathbf{Z}^{\pm}$ stands for the total amplitude of the Elsässer field at the point r.

Here we consider two possible NL couplings: first, one which is local in the frequency space so that only waves of the same frequency interact nonlinearly (model A). In this case $\mathbf{Z}^{\pm} = \mathbf{z}^{\pm}(\omega_j)$, the dissipation rate is independent of the way the energy is distributed and is determined essentially by the local frequency-dependent reflection rate. Although this model is not realistic (these are generally non-resonant interactions) it is helpful in understanding the more complex wave evolution that arises once nonlocal interactions are considered (model B). In the latter case $\mathbf{Z}^{\pm}$ stands for the total amplitude of the Elsässer field integrated over the whole spectrum, hence $\mathbf{Z}^{\pm} = \sqrt{\int_\Omega [|z^{\mp}(\omega)|^2/\omega\ d\omega]}$. The energy distribution among the modes influences the dissipation rate of all the waves. In particular, at a fixed total rms energy, dissipation is reduced if the energy of the higher frequency waves is comparable to the energy residing in the low frequency waves (flatter spectra) with respect to the case in which most of the energy is contained in the low frequency modes (steeper spectra) (Verdini et al. 2005). The equations become, after Fourier transform in time:

$$\mathbf{z}^{\pm\prime} - i\frac{\omega}{U \pm V_a}\mathbf{z}^{\pm} + \frac{1}{2}\frac{A'}{A}\frac{U \mp V_a}{(U \pm V_a)}\mathbf{z}^{\mp} + \frac{1}{2}\frac{\mathbf{z}^{-} - \mathbf{z}^{+}}{U \pm V_a} \times$$
$$\times \left[\frac{A'}{A}\left(V_a \mp \frac{1}{2}U\right) + \left(V_a' \mp \frac{1}{2}U'\right)\right] = -\frac{\mathbf{z}^{\pm}|\mathbf{Z}^{\mp}|}{L(U \pm V_a)} \tag{3}$$

for the corona, while for the photosphere and the cromosphere one gets:

$$\mathbf{z}^{\pm\prime} \mp i\frac{\omega}{V_a}\mathbf{z}^{\pm} + \frac{1}{2}\frac{V_a'}{V_a}\mathbf{z}^{\mp} = \mp\frac{\mathbf{z}^{\pm}|\mathbf{Z}^{\mp}|}{\rho^{1/4} L V_a} \tag{4}$$

after the substitution $z^{\pm} \rightarrow \rho^{1/4} z^{\pm}$ is performed to account for the systematic variation due to the density gradients.
The dissipative feature of the nonlinear terms can be shown multiplying eq.3 by the complex conjugate $\mathbf{z}^{\pm *}$ to obtain the evolution equations for the Elsässer energies at a given frequency $E^{\pm} \equiv \frac{1}{2}|\mathbf{z}^{\pm}(\omega)|^2$. On the RHS one gets $-|\mathbf{z}^{\pm}|^{\mathbf{2}}|\mathbf{Z}^{\mp}|/[(U \pm V_a)L]$, which is independent of the phase difference between the two fields and involves the total amplitude of the fluctuations. In the presence of a wind, energy flux as conserved quantity is replaced, for linear ly propagating waves, by the total wave action flux, which may be written as the difference between an outgoing and incoming flux. The inward wave action density vanishes at the Alfvén critical point X_c, so one may write $S^* = S_0^+ - S_0^- = S_c^+$, where the index c stand for the critical point, while the index 0 refers to the base of the layer, $+, -$ refer to outward/inward and S is wave action. Amplitude and the phase of the outward propagating Elsässer field ($\mathbf{z}^+$) at X_c define the natural boundary conditions, since the critical point is a regular singular point for the incoming wave equation, because phase velocity of the mode vanishes there: total wave action density is imposed and the amplitude and phase of $\mathbf{z}^-$ can be derived demanding regularity of the solutions at X_c. However, boundary conditions should be chosen to ensure an amplitude of the velocity field fluctuations summed over the whole spectrum of about 20 km/s at $1\ R_{\odot}$, with an assigned spectral distribution: this requires some trial and error since regularity of solutions is imposed at X_c.

The phenomenological turbulent length scale varies as $L(r) = L_0 \times \sqrt{A(r)}$ where $L_0 = 34,000$ km is imposed at $1\ R_{\odot}$ and corresponds to the average size of the supergranules. The waves are propagated forward from X_c (to Earth's orbit) and backwards (to the base of the Corona) by integration of eqs. 3. The conservation of the energy flux across the transition region allows one to determine the Elsässer fields below the discontinuity which are propagated back to the base of the photosphere using eqs. 4.

3. RESULTS

When nonlinear terms are taken into account the conserved quantities decrease with distance from the Sun because of the dissipative features of $NL^{\pm}$. To quantify the dissipation we plot the conserved quantity, computed at the top of the layer and normalized to its value at the base of the same layer ($\gamma = S^*_{top}/S^*_{bot}$), as a function of frequency for the local interaction model A (fig. 1). One can readly see that the most reflected waves are the most damped waves. Note that in the photosphere and cromosphere some signature of the peaks remain as remnants of the linear behavior.
One can then identify two ranges of frequencies which will be the driving modes for the dissipation in the nonlocal interaction model: $10^{-6}\ Hz < \omega < 510^{-3}\ Hz$ for the photosphere and the cromosphere, $\omega < 10^{-4}\ Hz$ for the subalfvénic corona. In fig. 2 the variation of

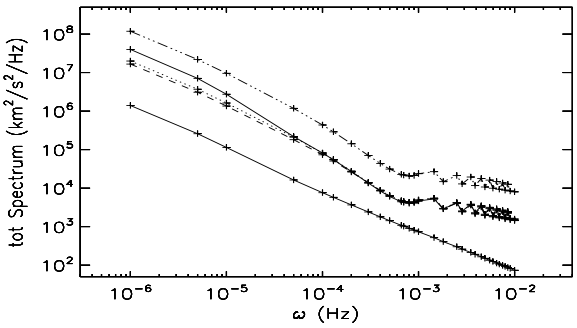

Figure 4. Total spectrum of the fluctuations (kinetic + magnetic energy per unit mass and frequency) calculated at five radial distances for model B. From the top to the bottom: Earth orbit (solid line), Alfvén critical point (dashed-triple dotted line), above the Transition Region ($1\ R_{\odot}$, at the base of the subalfvénic Corona, dotted line), below the Transition Region (dashed line) and the base of the Photosphere ($-2400\ km$, solid line, slope approximately equal to -1). Crosses indicate the frequencies chosen to describe the spectrum.

$S^*(r)/S^*_{bot}$ is plotted as function of r for the corona in the two models A (main figure) and B (subfigure) for the 32 frequencies forming the spectrum. According to fig. 1 the lowest frequency waves experience the biggest damping and the highest frequency waves are nearly not damped. If non local interaction are taken into account (subfigure), the highest frequency waves are damped at almost the same rate of the lowest frequency ones, which actually drive the dissipation by coupling into all the modes.

In fig. 3 the same plots are shown for the photosphere and the cromosphere. Here only four representative frequencies are shown. It is to noteworthy how nonlinear terms are more efficient in coupling the wave-evolution in this region. In fact, despite the smaller wave amplitude in this layer, the reflection is stronger for all the frequencies so that also the range of the driving modes is wider.
We now look at the spectrum evolution, including also the superalfvénic part of the corona, to the earth orbit. In this region the dissipation is higher for low frequency waves and vanishes at high frequency as in the subalfvénic corona. Again the driving modes are the low frequency waves ($\omega < 10^{-4}$ Hz) and the coupling among the different waves is strong in the nonlocal interaction model.

In the photosphere and in the cromosphere, the strong reflection rates inside the layer and the even stronger reflection at the transition region produce an almost equal amount of outward and inward propagating waves. Since there is basically no imbalance between the opposite propagating waves the dissipation acts on both z^+ and z^- at the same rate, the wave amplitude is too small and nonlinear coupling is too weak to overcome the the linear terms which then determine the waves evolution (even in the nonlocal interaction model). This allows one to correct the slope of the spectrum at the critical point in order

to start with a (almost) flat spectrum at the base of the photosphere. This has been carried out for all the models but results are shown only for model B in fig. 4. Most of the changes in the slopes occur in the cromosphere and photosphere. At high frequencies ($\omega > 10^{-3}$ Hz) the spectrum flattens and the peaks appear. At intermediate frequencies (210^{-4} Hz $< \omega < 10^{-3}$ Hz) the spectrum steepens while at low frequencies it remains almost unchanged. As the waves propagate further out in the atmosphere the spectrum does not evolve until the waves reach the superalvénic corona. There the intermediate-low frequency branch steepens while the high frequency part does not change.

Finally at Earth's orbit the spectrum may be divided into three branches: almost flat for $\omega < 510^{-5}$ Hz (slope approximately equal to -1), steeper for 510^{-5} Hz $< \omega < 610^{-4}$ Hz (slope approximately equal to -1.5) and flatter for $\omega > 610^{-4}$ Hz (average slope approximately equal to -0.4). In the linear case most of the evolution takes place in the photosphere and cromosphere (similar behavior) and in the subalfvénic corona where the spectrum slightly steepens at intermediate frequencies. In the superalfvénic corona finally the spectrum remains unchanged.

Given these results, it is clear that other, more complex, processes, must be acting on the fluctuations, including some form of parallel cascade to iron out the high-frequency remnants of the photospheric-coronal transmission. We plan to investigate these effects using a more realistic model of NL interactions in the near future.

ACKNOWLEDGEMENTS

This work was completed while the authors were participating in the NSF funded IPAM program "Grand Challenge Problems in Computational Astrophysics" at UCLA. This work has also been partially supported by tthe Research Training Network (RTN) Theory, Observation, and Simulation of Turbulence in Space Plasmas, funded by the European Commission (contract HPRN-CT-2001-00310). MV acknowldeges support from NASA.

REFERENCES

Casalbuoni, S., Del Zanna, L., Habbal, S. R., & Velli, M. 1999, J. Geophys. Res., 104, 9947

Dmitruk, P. & Matthaeus, W. H. 2003, ApJ, 597, 1097

Dmitruk, P., Matthaeus, W. H., Milano, L. J., & Oughton, S. 2001a, Physics of Plasmas, 8, 2377

Dmitruk, P., Matthaeus, W. H., Milano, L. J., et al. 2002, ApJ, 575, 571

Dmitruk, P., Milano, L. J., & Matthaeus, W. H. 2001b, ApJ, 548, 482

Heinemann, M. & Olbert, S. 1980, J. Geophys. Res., 85, 1311

Hollweg, J. V. 1978, Sol. Phys., 56, 305

Hollweg, J. V., Jackson, S., & Galloway, D. 1982, Sol. Phys., 75, 35

Kopp, R. A. & Holzer, T. E. 1976, Sol. Phys., 49, 43

Leroy, B. 1980, A&A, 91, 136

Lou, Y. & Rosner, R. 1994, ApJ, 424, 429

Mangeney, A., Grappin, R., & Velli, M. 1991, Advances in Solar System Magnetohydrodynamics (Priest, E. R. and Hood, A. W.), 327

Matthaeus, W. H., Smith, C. W., & Oughton, S. 1998, J. Geophys. Res., 103, 6495

Matthaeus, W. H., Zank, G. P., Oughton, S., Mullan, D. J., & Dmitruk, P. 1999, ApJ, 523, L93

Munro, R. H. & Jackson, B. V. 1977, ApJ, 213, 874

Oughton, S., Dmitruk, P., & Matthaeus, W. H. 2004, Physics of Plasmas, 11, 2214

Oughton, S., Matthaeus, W. H., Dmitruk, P., et al. 2001, ApJ, 551, 565

Similon, P. L. & Zargham, S. 1992, ApJ, 388, 644

Velli, M. 1993, A&A, 270, 304

Velli, M., Grappin, R., & Mangeney, A. 1991, Geophys. Astrophys. Fluid Dynamics, 62, 101

Verdini, A., Velli, M., & Oughton, S. 2005, submitted

Zank, G. P., Matthaeus, W. H., & Smith, C. W. 1996, J. Geophys. Res., 101, 17093